

A mouse model for polycystic kidney disease through a somatic in-frame deletion in the 5' end of *Pkd1*

PG Starremans^{1,4}, X Li^{1,4}, PE Finnerty¹, L Guo¹, A Takakura¹, EG Neilson^{2,3} and J Zhou¹

¹Department of Medicine, Renal Division, Harvard Institutes of Medicine, Brigham and Women's Hospital and Harvard Medical School, Boston, Massachusetts, USA; ²Department of Medicine, Vanderbilt University, Nashville, Tennessee, USA and ³Department of Cell and Developmental Biology, Vanderbilt University, Nashville, Tennessee, USA

Autosomal dominant polycystic kidney disease, a leading cause of end-stage renal disease in adults, is characterized by progressive focal cyst formation in the kidney. Embryonic lethality of *Pkd1*-targeted mice limits the use of these mice. Here we developed a floxed allele of *Pkd1* exons 2–6. Global deletion mutants developed polyhydramnios, hydrops fetalis, polycystic kidney and pancreatic disease. Somatic *Pkd1* inactivation in the kidney was achieved by crossing *Pkd1*^{flox} mice with transgenic mice expressing Cre controlled by a γ -glutamyltranspeptidase promoter. These mutants developed cysts in both proximal and distal nephron segments and survived for about 4 weeks. Somatic loss of heterozygosity was shown in a reporter mouse strain to cause cystogenesis. Some cysts in young mice are positive for multiple tubular markers and a mesenchymal marker, suggesting a delay in tubular epithelial differentiation. A higher cell proliferation rate was observed in distal nephron segments probably accounting for the faster growth rate of distal cysts. Although we observed an overall increase in apoptosis in cystic kidneys, there was no difference between proximal or distal nephron segments. We also found increased cyclic AMP, aquaporin 2 and vasopressin type 2 receptor mRNA levels, and apical membrane translocation of aquaporin 2 in cystic kidneys, all of which may contribute to the differential cyst growth rate observed. The accelerated polycystic kidney phenotype of these mice provides an excellent model for studying molecular pathways of cystogenesis and to test therapeutic strategies.

Kidney International (2008) **73**, 1394–1405; doi:10.1038/ki.2008.111; published online 2 April 2008

KEYWORDS: ADPKD; cystogenesis; polycystin; conditional knockout mouse

Correspondence: J Zhou, Department of Medicine, Renal Division, Harvard Institutes of Medicine, Brigham and Women's Hospital and Harvard Medical School, Room 522, 4 Blackfan Circle, Boston, Massachusetts 02115 USA. E-mail: zhou@rics.bwh.harvard.edu

⁴These authors contributed equally to this work

Received 27 February 2007; revised 22 September 2007; accepted 24 October 2007; published online 2 April 2008

Autosomal dominant polycystic kidney disease (ADPKD) is the most common inherited kidney disorder, with an average occurrence of 1:500–1:1000 people and accounting for >5% of patients with end-stage renal failure in Europe and the United States.¹ ADPKD is characterized by focal formation of multiple cysts in the kidneys, in the liver in ~50% of cases, and much less frequently in the pancreas. Cardiovascular abnormalities, including hypertension, mitral valve prolapse, and intracranial aneurysms, are also often recognized. ADPKD is caused by mutations in *PKD1* and *PKD2* genes encoding polycystin-1 and 2 (PC1 and PC2). PC1 and PC2 function as a mechanosensitive receptor-channel protein complex and mediate G-protein and Ca²⁺ signaling.^{2,3}

Every cell in an ADPKD patient carries an inherited mutation in either the *PKD1* or *PKD2* gene, yet focal cysts form in only ~5% of nephrons. Reeders⁴ proposed a 'two-hit' hypothesis to explain the focal nature of cyst development: a germline mutation in one of the two copies ('alleles') of, for example, *PKD1* in a given cell is not sufficient to alter the phenotype of that cell and initiate cyst formation because the second allele is functioning normally. Cystogenesis occurs when a somatic mutation knocks out the 'normal' allele so that one allele has a germline mutation ('first hit'), the other has a somatic mutation ('second hit'), neither allele is functional, and no PC function remains. A cyst then forms through proliferation of the cell that has received two 'hits.' The hypothesis predicts that the number of cysts will increase during life as the somatic or second hits accumulate. This hypothesis has since received support from studies in renal cysts⁵ and liver cysts⁶ using human tissues with ADPKD.

Using gene targeting, a powerful tool for studying gene function *in vivo*, inactivation of mouse *Pkd1* and *Pkd2*, including *Pkd1*^{del34},⁷ *Pkd1*^{del43–45},⁸ *Pkd1*^{null},⁹ *Pkd1*^{del17–21βgeo},¹⁰ and *Pkd2*,¹¹ resulted in similar phenotypes. In homozygotes, kidney development proceeds normally until embryonic day 15.5, at which time point cystic dilatation of renal tubules is evident, as is cystic degeneration in the pancreas,^{7,9} which is consistent with the 'two-hit' hypothesis. All homozygous mice develop polyhydramnios and hydrops fetalis.^{7,9} Whereas defects in skeletal development have been described for *Pkd1*

mutants,^{9,10} *Pkd2*-targeted mice develop laterality defects.¹² Mice with a heterozygous mutation of *Pkd1*, however, only develop scattered renal and hepatic cysts late in life.¹³ The slow rate of cyst development in *Pkd1* heterozygotes was hypothesized to be the result of the slow development of somatic second hits in mice.¹³

Conventional gene targeting has provided us valuable clues about the role of PC1 and PC2 in development;^{7–11} however, it has been less effective in elucidating the physiological or pathophysiological processes that occur later in life for the following reasons. First, inactivation of a developmentally important gene, such as *Pkd1*, resulted in perinatal lethality, excluding the possibility of functional analysis in adult life. Second, conventional gene-targeting technology is unable to introduce mutations in a time- and location-specific manner.

The *Cre-loxP* site-specific recombination system has been used successfully to produce mice with tissue- and time-specific deletions.¹⁴ By crossing ‘floxed’ mice with transgenic mice expressing the *Cre* recombinase in the desired time- and/or tissue-specific manner, one can achieve conditional gene inactivation. This approach was used recently to develop a conditional model in which somatic *Pkd1* inactivation was under the control of MMTV.*Cre*.¹⁵ Although mice were created successfully, only scattered cysts were observed in mice at 20 weeks of age. The lack of a polycystic kidney phenotype and the length of time needed to develop scattered cysts limit the usefulness of this model for phenotypic and experimental studies of ADPKD.

In this study, we developed two new *Pkd1*-knockout mouse models simultaneously with using *Cre-loxP* technology. These mice develop striking polycystic kidney pathology. Disruption of the *Pkd1* gene in a time- and tissue-specific manner yielded direct evidence supporting the two-hit hypothesis.

RESULTS

Generation of the *Pkd1* conditional knockout mouse

A *Pkd1* conditional construct was designed to study the effects of loss of PC function after birth. A loxP-flanked *neomycin* selection cassette was inserted into the *EcoRI* site located 1.2 kb upstream of exon 2, and a third loxP site was placed in intron 6 (Figure 1a). Homologous recombinants were identified by Southern blotting using a 5' probe. Two independently targeted embryonic stem cell clones were injected into C57BL/6J blastocysts. The resulting chimeric mice, with >90% of the agouti coat, were crossed with C57BL/6 and BALB/c mice to produce F1 progeny with germline transmission.

The offspring with germline transmission were crossed with mice carrying a germline *Cre* transgene (*Prm.Cre*). The *Cre* recombinase targets random combinations of any of the three available loxP sites and results in four possible recombinations, two of which are desirable events (Figure 1b). One leads to complete deletion of the region between the two outlying loxP sites, creating a conventional knockout,

dubbed ‘*Pkd1*^{del2–6}’. The other leads to removal of only the *neomycin* cassette, which creates what is commonly called a ‘floxed’ allele. The latter is used for generating conditional knockouts by crossing with a transgenic mouse expressing a tissue-specific *Cre* recombinase.

The design of the *Pkd1* conditional targeted construct was expected to result in deletion of exons 2 through 6, which is an in-frame deletion. Reverse transcriptase-polymerase chain reaction on RNA isolated from kidneys with primers specific for exons 1(KO-F), 2 (F27), 5(R37), 10 (R104/F201), and 11(R201) (Figure 1a, ‘floxed’ allele) showed that the *Pkd1* transcript present in our conventional mutants lacks not only exons 2 through 6, but also exon 7 (Figure 1c). This alternative splicing event resulted in a transcript with a stop codon at the beginning of exon 8 (Figure 1c).

To investigate whether these mutant transcripts produced stable products, we examined the expression levels of the *Pkd1* protein in kidney lysates from *Pkd1*^{del2–6} homozygotes and heterozygotes, and compared them with that of wild-type littermates using a monoclonal antibody, 7e12, directed against the N-terminal region of PC1. A band of ~460 kDa was detected in both the wild-type and heterozygous newborn kidneys, but it was absent in homozygous *Pkd1*^{del2–6} mutants (Figure 1d, left). PC2 appears to be expressed normally, although protein levels in the *Pkd1*^{del2–6} homozygotes appeared to be slightly decreased (Figure 1d, right). PC1 and PC2 directly interact through the putative coiled-coil domains in their C-termini.¹⁶

It has been reported that the rate of cell proliferation increases in ADPKD kidney epithelia, which may be a result of decrease of p21 in polycystic kidneys.¹⁷ Similar to our *Pkd1*^{null/null} mutants,¹⁸ we found an decrease in the expression of cyclin-dependent kinase inhibitor p21 in the kidneys of newborn *Pkd1*^{del2–6/del2–6} mice, as compared with that in their respective wild-type littermates (Figure 1e). However, p27 expression in homozygous *Pkd1*^{del2–6} kidneys was not altered significantly (Figure 1e).

Rapid progression of kidney cysts in homozygous *Pkd1*^{del2–6} pups

To investigate whether deletion of exons 2–6 of the *Pkd1* gene would result in functional inactivation of PC1, we intercrossed *Pkd1*^{del2–6} mice to produce homozygous *Pkd1*^{del2–6/del2–6} offspring. From our previous studies, we know that homozygous inactivation of *Pkd1* results in embryonic lethality; we therefore expected that *Pkd1*^{del2–6/del2–6} offspring were unlikely to be viable. To our surprise, ~50% of the homozygous *Pkd1*^{del2–6/del2–6} mice survived to birth (Table 1).

The survival rate for mice homozygous for *Pkd1*^{del2–6} was much higher than that of mice homozygous for the previously described *Pkd1*^{null} mutants.⁹ Virtually all homozygous *Pkd1*^{del2–6} pups died on the day of birth, whereas homozygous *Pkd1*^{null} mutants died as early as E13.5, with a peak between E14.5 and E16.5,⁹ although in very rare cases, they survived longer. *Pkd1*^{del2–6/del2–6} mutants (Figure 2b) displayed a comparable cystic phenotype as *Pkd1*^{null/null}

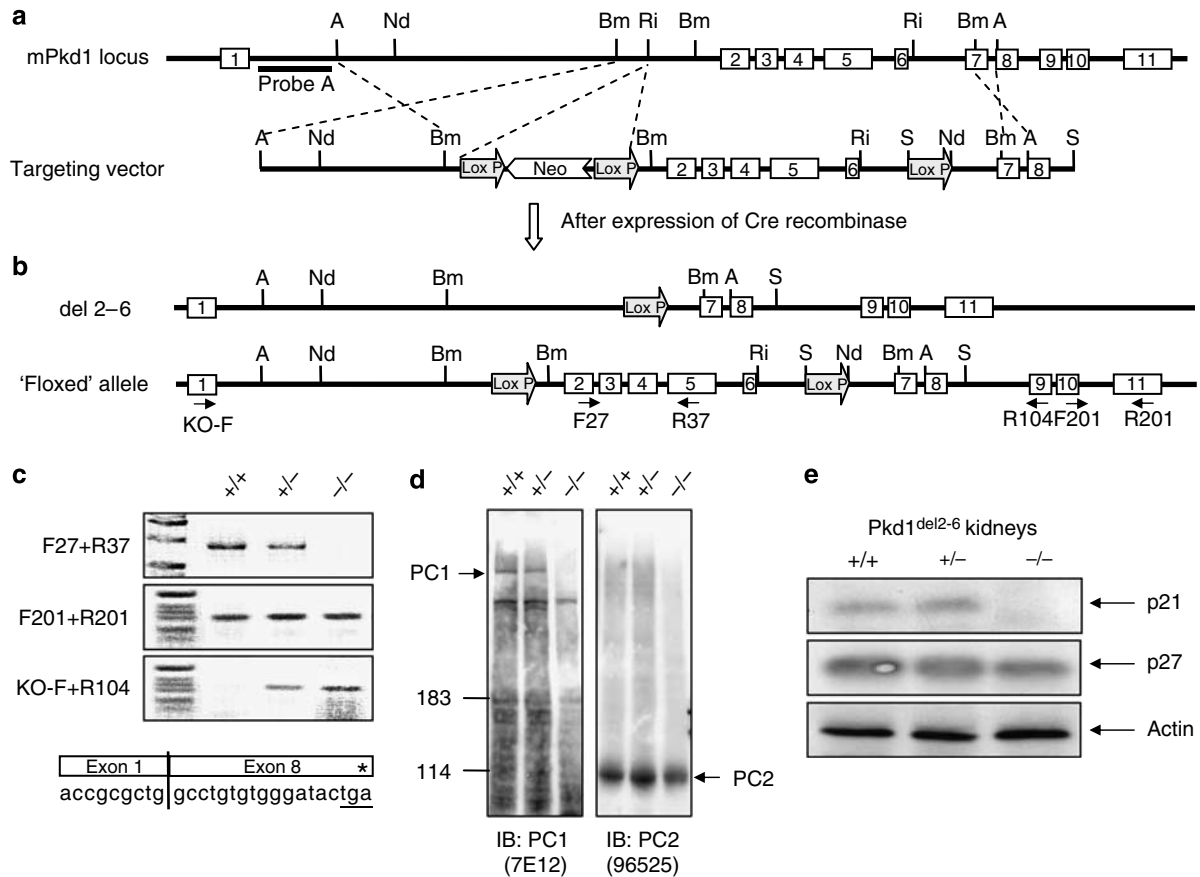


Figure 1 | Generation of the *Pkd1* conditional targeted mice. (a) Structure of the wild-type *Pkd1* allele and the targeting strategy resulting in 'floxed' exons 2–6 preceded by a 'floxed' neomycin cassette. Restriction sites: A, *AvrII*; Bm, *BamHI*; Nd, *NdeI*; Ri, *EcoRI*; S, *SpeI* (b) The two desired recombination events after expression of *Cre* out of four possible recombinations. Genotyping primers (KO-F/R104, F27-R37, F201-R201) are indicated below the 'floxed' allele. (c) Reverse transcriptase-polymerase chain reactions showing the splicing events for exons 2–5 (F27–F37), exon 10–11 (F201 + R201), and exon 1–9 (KO-F–R104) in wild-type, heterozygous, and homozygous mice. Shown below is the sequence of the *Pkd1* transcript after recombination, resulting in a stop codon in exon 8. (d) Immunoblots of wild type, heterozygote, and homozygote kidney lysates for PC1 (left blot) and PC2 (right blot). (e) Levels of p21 and p27 expression in kidneys from wild type, heterozygous, and homozygous *Pkd1*^{del2-6} mice. Actin was used as a control.

Table 1 | Newborn survival rate for homozygous *Pkd1*^{del2-6/del2-6} or *Pkd1*^{null/null} mice

Mutation	No. of litters	No. of pups	No. of -/-	Expected no. of -/-	Survival (%)
C57/B6 null	17	143	4	36	11.1
C57/B6 129SvEv Del2-6	46	323	41	81	50.6

mutants (Figure 2c). A large percentage of glomeruli also develop cysts in both *Pkd1*^{del2-6/del2-6} (Figure 2e) and *Pkd1*^{null/null} (Figure 2f) homozygotes.

Timed pregnancies (Table 2) were set up, and 25 *Pkd1*^{del2-6} homozygotes were examined histologically for renal cystic lesions. At E15 and E17, the cyst size in *Pkd1*^{del2-6} kidneys was comparable to that of *Pkd1*^{null} kidneys at the respective stages. The homozygous *Pkd1*^{del2-6} pups surviving to birth exhibited the same phenotype as documented previously for other *Pkd1* homozygous mutations, with polyhydramnios and systemic edema.^{7,9} Onset of the cystic phenotype in *Pkd1*^{del2-6} homozygous embryos occurred at the same stage (E15.5) as reported for the *Pkd1*^{del34} and *Pkd1*^{null} mutants^{7,9} (data not shown).

Somatic inactivation of the normal allele of *Pkd1* and the two-hit hypothesis

To achieve conditional inactivation of *Pkd1* in kidney, we bred our *Pkd1*^{flox} mice with a transgenic mouse in which *Cre* expression was driven by a promoter fragment of γ -glutamyltranspeptidase (γ Gt). γ Gt is expressed and regulated in a tissue-specific manner, and is known to be present in bile ducts, kidney, intestine, and other organs involved in secretion. The γ Gt.*Cre* transgene is known to be expressed in the kidney proximal tubule.¹⁹ To evaluate the effects of the somatic inactivation of *Pkd1* and the role of compound heterozygous mutations on cyst formation, we crossed γ Gt.*Cre*:*Pkd1*^{+ /flox} with *Pkd1*^{null / +} mice to produce γ Gt.*Cre*:*Pkd1*^{null / flox} offspring. The expected Mendelian ratios

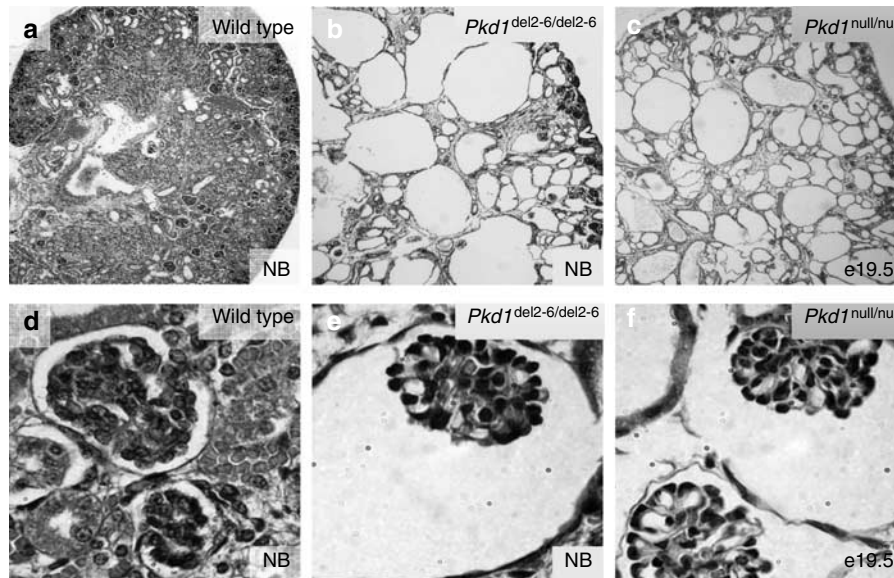


Figure 2 | Phenotype of a new *Pkd1* mutation lacking a neomycin cassette. Histological comparison of kidney phenotypes in hematoxylin–eosin-stained sections (original magnification $\times 25$) from newborn wild-type (a) newborn *Pkd1*^{del2-6/del2-6} (b), and a rare *Pkd1*^{null/null} pup surviving until E19.5 (c). (d–f) Glomeruli (original magnification $\times 400$) from the same sections used in (a–c) showing cyst formation in glomeruli from (e) newborn *Pkd1*^{del2-6/del2-6} and (f) *Pkd1*^{null/null}.

Table 2 | *Pkd1*^{del2-6/del2-6} timed pregnancies

Stage	No. of pups	No. of –/–	Expected –/–	Survival (%)
E15.5 days	73	20	18	100
E17.5 days	21	5	5	100

were observed for live-born progeny of all possible genotypes, indicating that no embryos in any group died during embryogenesis. Although no cystic phenotype was observed in heterozygous mice with γ Gt.Cre:*Pkd1*^{+ /null} (Figure 3a) or γ Gt.Cre:*Pkd1*^{+ /flox} (Figure 3b) genotype, γ Gt.Cre:*Pkd1*^{null/flox} mice had severe cystic lesions at 10 days (Figure 3c), with progressive increase in severity over time (Figure 3d). However, glomerular cysts seen in *Pkd1*^{null/null} and *Pkd1*^{del2-6/del2-6} mice were not observed in γ Gt.Cre:*Pkd1*^{null/flox} mice (Figure 3e) even at 26 days (Figure 3f). Most γ Gt.Cre:*Pkd1*^{null/flox} offspring died before 1 month of age. These data confirm the ‘two-hit’ theory that somatic inactivation of the second *Pkd1* allele in mice carrying a heterozygous germline mutation leads to a dominant PKD phenotype.

Characterization of cyst origins in γ Gt.Cre:*Pkd1*^{flox/flox}

To further characterize the nature of the cysts, we fixed and sectioned kidneys from 10-day-old γ Gt.Cre:*Pkd1*^{flox/flox} (Figure 4d–f) mice and their *Pkd1*^{flox/flox} littermates lacking *Cre* (Figure 4a–c). Histological analysis showed an obvious cystic phenotype in the kidneys of *Cre*-carrying animals (Figure 4d). We subsequently stained these sections with tubular markers *Lotus tetragonolobus* agglutinin (LTA) (Figure 4b and e; Figure S1a, c, d, and f), *Dolichos biflorus*

agglutinin (DBA) (Figure 4c and f; Figure S1b, c, g, and i), and anti-Tamm–Horsfall protein (THP) (Figure S1e, f, h, and i), which selectively stain the proximal tubule, the collecting tubule/duct segments, or the thick ascending limbs of Henle’s loop, to identify the tubular origin of a particular cyst. We found that cysts in γ Gt.Cre:*Pkd1*^{flox/flox} kidneys can originate from either proximal or distal tubular segments, with the larger cysts being mainly distal rather than proximal in origin (Figure 4c; Figure S1a–i). These findings expand upon the observation that γ Gt.Cre is expressed in mouse kidney cortex, since specific tubular segments were not characterized in that study.¹⁹

To determine whether collecting tubule cysts were secondary to proximal tubule cysts, or were the result of *Cre* expression in these tubules, we generated γ Gt.Cre:*DsRed*:*Pkd1*^{flox/flox} mice by introducing a *DsRed* reporter transgene into the γ Gt.Cre:*Pkd1*^{flox/flox} background. The *DsRed* transgene is preceded by a floxed sequence that prevents its expression. Excision of the floxed sequence by a *Cre* recombinase is required for constitutional expression of fluorescent protein. Presence of *DsRed* could be clearly detected in most cortical tubule segments in frozen tissue sections from control γ Gt.Cre:*DsRed*:*Pkd1*^{flox/+} mice (not shown). Because of the poor morphology of frozen cystic kidney sections from γ Gt.Cre:*DsRed*:*Pkd1*^{flox/flox} mice, we stained formalin-fixed, paraffin-embedded, kidney sections with an fluorescein isothiocyanate-coupled anti-red fluorescent protein (RFP) antibody. *DsRed* protein (green) could be detected in the epithelial cells of cysts derived from the proximal tubule (Figure 5a–c), the thick ascending limb of Henle’s loop (TAL) (Figure 5d–f), and the collecting tubules (Figure 5g–i). These results indicate that the γ Gt promoter

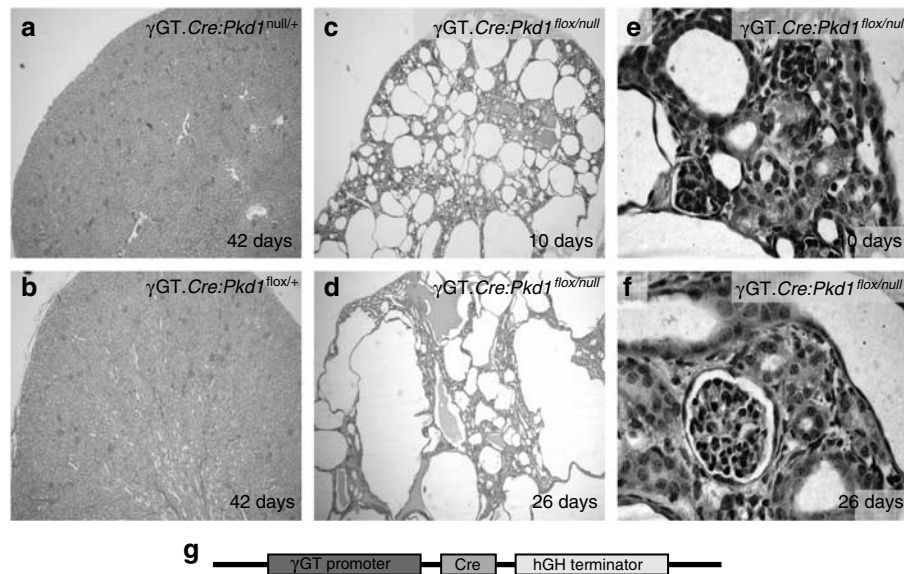


Figure 3 | Somatic inactivation of a *Pkd1* allele. Histological comparison of kidney phenotype in hematoxylin–eosin-stained sections from $\gamma\text{Gt.Cre:Pkd1}^{\text{null/+}}$ (a) and $\gamma\text{Gt.Cre:Pkd1}^{\text{flox/+}}$ (b) heterozygote control mice (42 days old), showing no signs of cysts versus $\gamma\text{Gt.Cre:Pkd1}^{\text{flox/null}}$ compound heterozygotes at 10 days (c) or 26 days (d) of age with a clear progressive cystic kidney phenotype (original magnification $25\times$). (e, f) Original magnification $\times 400$ showing absence of glomerular cysts in $\gamma\text{Gt.Cre:Pkd1}^{\text{flox/null}}$ kidneys at 10 (e) or 26 days (f).

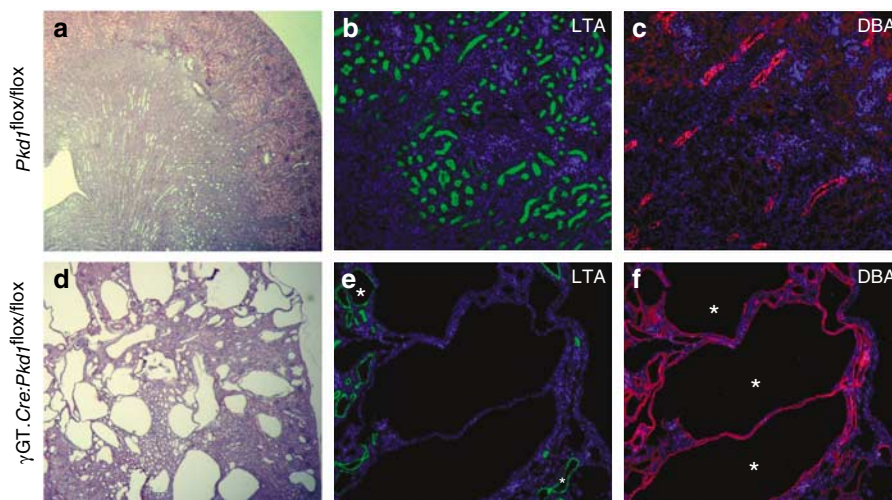


Figure 4 | Effects of $\gamma\text{Gt.Cre}$ as the inducer of cyst formation. Comparison of kidney sections of 10-day-old *Pkd1*^{flox/flox} controls (a–c) and $\gamma\text{Gt.Cre:Pkd1}^{\text{flox/flox}}$ -knockout mice (d–f). (a, d) Hematoxylin–eosin (original magnification $\times 25$) (b, e) LTA staining (green) of control and knockout sections showing (dilated) tubules and cysts of proximal tubule origin. (c, f) DBA staining (red) of control and knockout sections showing (dilated) tubules and cysts of distal/collecting tubule origin. Asterisks indicate cysts (blue, DAPI; original magnification $\times 100$).

fragment is active in both proximal and distal nephron segments.

Distal tubular cysts progress at a faster rate than cysts of proximal tubule origin

Most of the larger cysts were located in the more medullary regions of the $\gamma\text{Gt.Cre:Pkd1}^{\text{flox/flox}}$ kidneys. We therefore investigated the tubular origins of these cysts in relationship to their size and progression rate. We co-stained kidney sections of 16 different animals ranging in age from 3 to 26 days for proximal (LTA) and distal (collecting tubule/ducts)

(DBA) tubular markers using directly labeled lectins to avoid the cross-reactions of secondary detection methods. Using fluorescence microscopy, we determined the number and origin of the cysts in at least three fields on two separate sections per animal. The relative cyst sizes were subsequently measured with Image-Pro Plus software. The rate of cyst enlargement in relationship with their origin (either proximal or distal) was documented and compared. Interestingly, the size of distal tubule cysts increased much more than the proximal tubule cysts (Figure 6a). Furthermore, after 12–15 days of age, the proximal tubule cysts did not increase in size

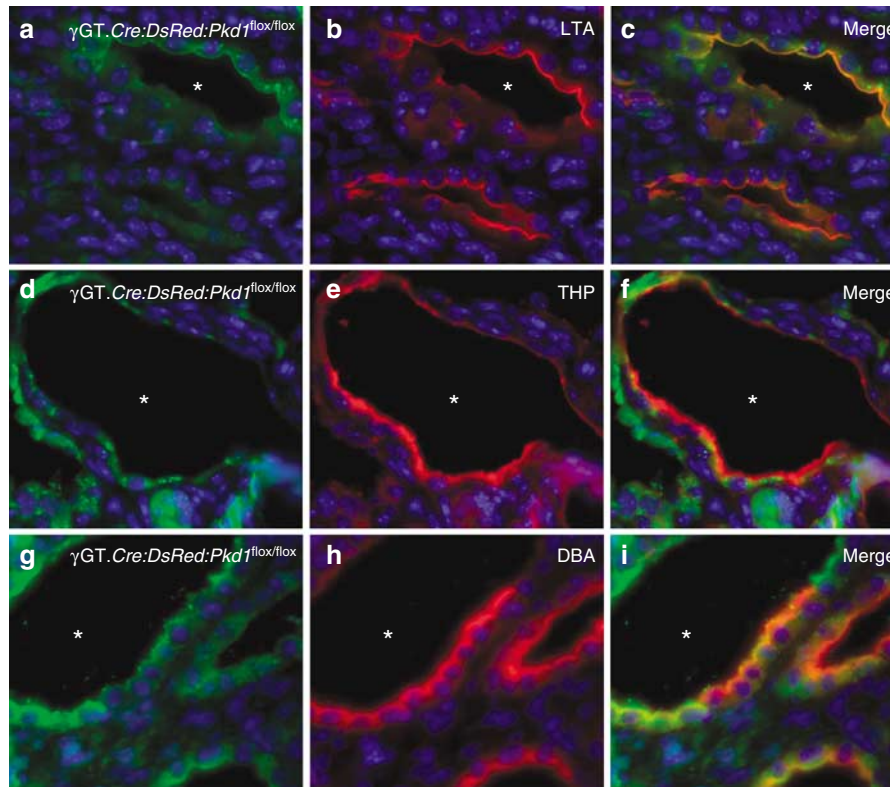


Figure 5 | γ Gt.Cre is active in cysts of both proximal and distal tubule origin in γ Gt.Cre:DsRed:Pkd1^{fllox/fllox} mouse kidneys at 27 days of age. (a–c) Co-staining for DsRed and LTA (b) indicating expression of the Cre recombinase in cysts (*) of proximal tubule origin (c). (d–f) Co-staining for DsRed and THP (e) indicating expression of the Cre recombinase in cysts (*) derived from the thick ascending limb of Henle’s loop (f). (g–i) Co-staining for DsRed and DBA (h) indicating expression of the Cre recombinase in cysts (*) of distal/collecting tubule origin (i) (blue, DAPI; original magnification \times 400).

and either regressed or completely disappeared, leaving mostly large cysts of distal tubule origin, which greatly increased the DBA:LTA cyst size ratio to \sim 70-fold (Figure 6b). A decrease in the total number of cysts was also noted, whereas the number of cysts of different origin per observed field remained largely constant, with an equal number of cysts expressing proximal or distal tubule markers. This decrease in the total number of cysts, combined with an overall increase in kidney volume, would thus account for the increase in the size of the individual distal tubular cysts (Figure 6c). Additionally, in animals younger than 12 days of age, up to 20% of cysts double labeled for DBA and LTA (Figure 6d). In older animals, however, no cysts expressed more than one marker.

The role of apoptosis and cell proliferation in cyst growth

To determine the role of apoptosis in the differential growth rates of cysts, we performed terminal uridine deoxynucleotidyl transferase dUTP nick-end labeling (TUNEL) staining on kidney sections from both cystic and control mice at 3, 5, 7, 13, 15, 23, and 26 days of age. At all time points investigated, normal controls (Figure S2a–c) showed little or no evidence of apoptosis, whereas many TUNEL-positive cells could be observed in their cystic littermates (Figure S2d–f).

However, no differences were observed between cysts in cortex or medulla of the kidney.

Since TUNEL staining detects breaks or ‘nicks’ in double-stranded DNA that can arise from sources other than apoptosis, we used a complementary assay for apoptosis, by detecting the cleavage of caspase 3. We co-stained kidney sections from 2-day-old cystic mice (Figure 7a–l) and their healthy littermates (Figure 7m–r) with an antibody to cleaved caspase 3 and a tubular marker, either LTA (Figure 7a–c, g–i and m–o) or DBA (Figure 7d–f, j–l and p–r). Both normal-looking tubules and cysts in γ Gt.Cre:Pkd1^{fllox/fllox} mice showed increased number of cells positive for cleaved caspase 3, indicating commitment to apoptosis. This increase, however, is similar between tubules and cysts of either proximal or distal origins. In contrast, cleaved caspase 3 was not detected in the normal kidneys.

To investigate the contribution of cell proliferation in the differential growth rates of cysts, we used kidney sections from 2-day-old cystic mice (Figure 8a–f) and their healthy littermates (Figure 8g–l), and co-stained for proliferating-cell nuclear antigen with either LTA (Figure 8a–c, g–i) or DBA (Figure 8d–f, j–l). We observed high levels of proliferation in the nephrogenic zone and outer medulla, where elongation of the Henle’s loop occurs,²⁰ and lower levels of proliferation in

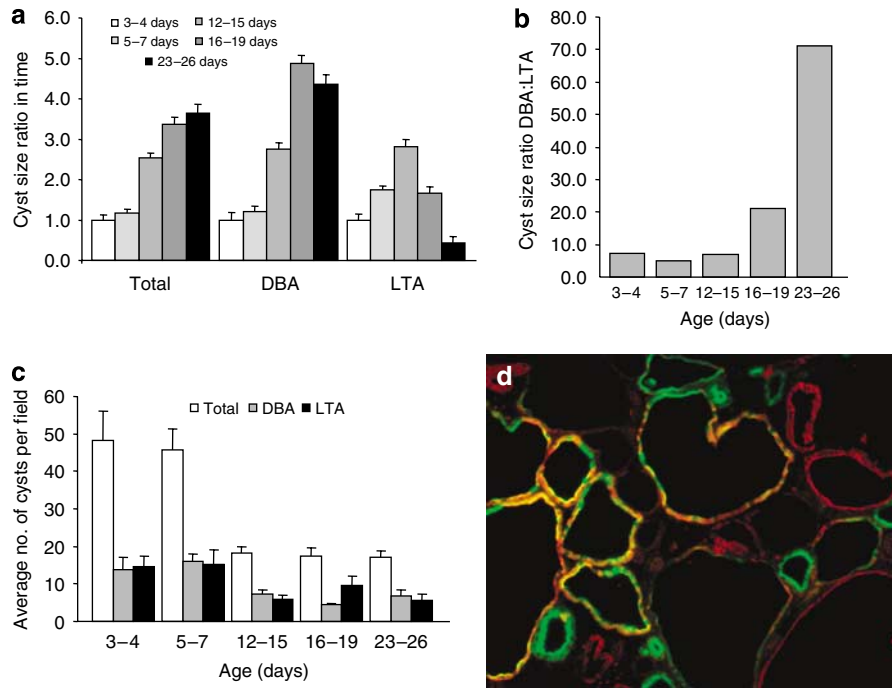


Figure 6 | Cysts of proximal and distal origin develop at different rates. (a) Average progression of cyst size in five age groups. Each group included four animals. The average cyst size of all cysts is compared with that of cysts of either distal or proximal tubule origin. A total number of ~1100 cysts were observed. (b) Plot of the ratio of DBA:LTA cyst size in five age groups. (c) Graph showing the average total number of cysts per counted field versus those of proximal or distal origin for five age groups. (d) Kidney section of a 7-day-old $\gamma\text{Gt.Cre:Pkd1}^{\text{flox/flox}}$ animal stained for LTA (green) and DBA (red) showing (dilated) tubules positive for both tubular markers (not seen in wild-type littermates), implying lack of terminal maturation.

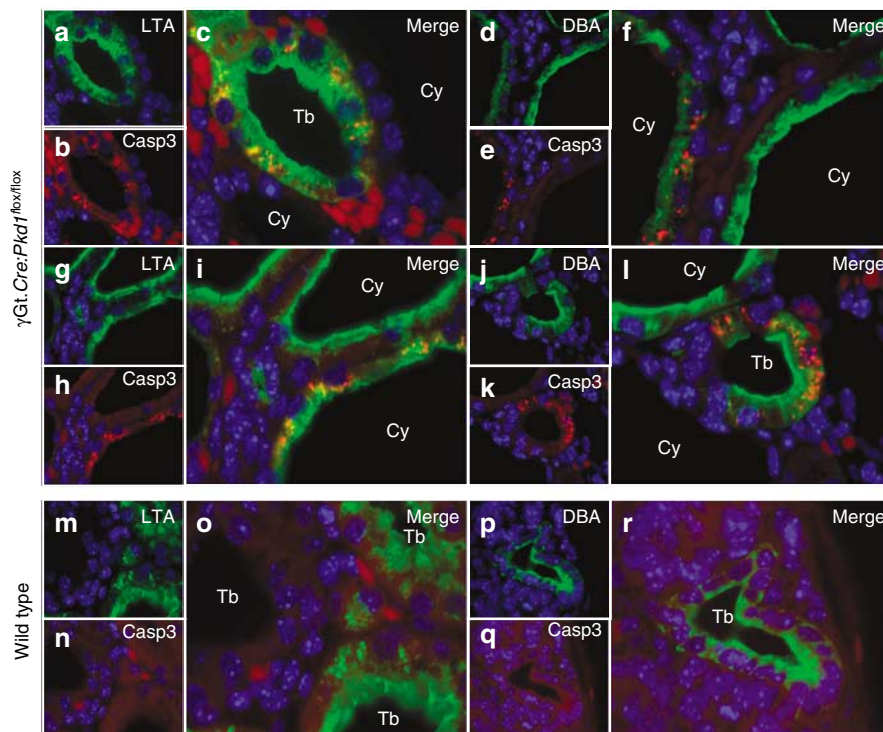


Figure 7 | Apoptosis in cysts and normal-looking tubules of proximal and distal origin in kidneys of 2-day-old $\gamma\text{Gt.Cre:Pkd1}^{\text{flox/flox}}$ mice. Co-staining for either LTA (a, c, g, i, m, o) or DBA (d, f, j, l, p, r) with cleaved caspase 3 (b, c, e, f, h, i, k, l, n, o, q, r) showing apoptosis in both cysts (d-f, g-i) and in normal-looking tubules (a-c, j-l) in $\gamma\text{Gt.Cre:Pkd1}^{\text{flox/flox}}$ kidneys versus normal controls (m-r) (blue, DAPI; original magnification $\times 1000$; cysts indicated by 'Cy', tubules indicated by 'T').

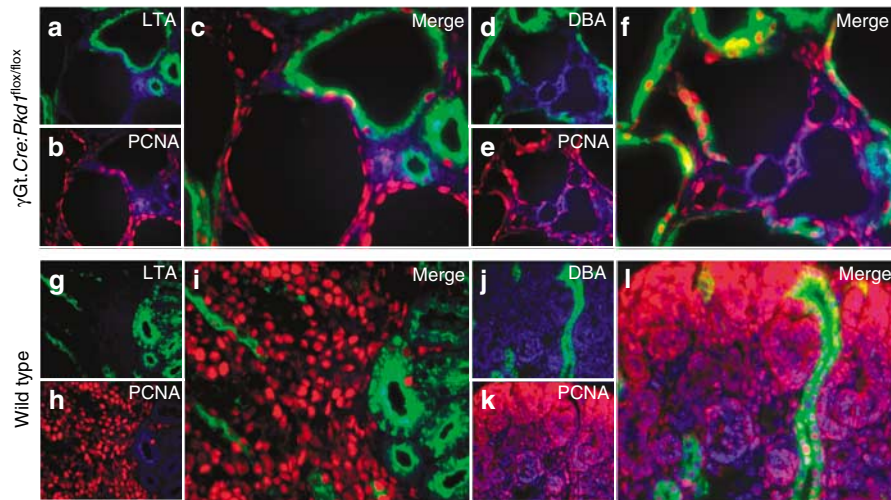


Figure 8 | Increased cell proliferation in the medullary kidney areas of 2-day-old γ Gt.Cre:*Pkd1*^{flox/flox} mice. Co-staining for either LTA (a, c, g, i) or DBA (d, f, j, l) with proliferating-cell nuclear antigen (b, c, e, f, h, i, k, l) showing large number of proliferating cells in the nephrogenic zone and distal tubular segments of both γ Gt.Cre:*Pkd1*^{flox/flox} (a–f) and normal kidneys (g–l) (blue, DAPI; original magnification $\times 1000$).

tubules positive for either LTA or DBA in wild-type littermates. In cystic kidneys, high levels of proliferation were seen in DBA-positive tubules (Figure 8d–f and j–l), in addition to the nephrogenic zone. No difference in proliferation was seen in LTA-positive tubules between wild-type and cystic kidneys (Figure 8a–c and g–i).

cAMP and cystogenesis

Changes in intracellular cAMP level could lead to changes in transcription and protein expression of cAMP-responsive proteins such as aquaporin 2 (AQP2) and the vasopressin V2 receptor (V2R). Moreover, AQP2 is known to translocate from the sub-apical domain to the apical membrane in response to increase in cAMP level. Therefore, we co-stained kidney sections from cystic mice with AQP2 and LTA (Figure 9a–c), or DBA (Figure 9d–f). Whereas AQP2 was located intracellularly in normal-looking tubules (Figure 9b and c, arrowhead), it was found in the apical membrane of large DBA-positive cysts (Figure 9b and c, arrows). No AQP2 signal was detected in LTA-positive cysts (Figure 9a–c, asterisk). We also measured cAMP levels in kidneys from both cystic animals and wild-type littermates, which revealed 20-fold increase in cAMP levels in cystic kidneys when compared with those in wild-type kidneys (Figure 9g). Using real-time PCR, we found a fivefold increase for AQP2, and a sevenfold increase for V2R at the mRNA expression level in cystic kidneys when compared with normal controls (Figure 9h and i).

DISCUSSION

In-frame deletion of *Pkd1* results in a null allele

In this study, we report the creation of a new conventional (*Pkd1*^{del2–6}) and conditional (*Pkd1*^{flox}) *Pkd1*-knockout mouse model. The design of the targeting strategy allowed us to create an in-frame deletion in the *Pkd1* gene and to study the

effects of PC1 lacking the leucine-rich repeat, the WSC homology domain, the first PKD domain, and the c-type lectin-binding motif in the extracellular domain. It was interesting to discover that an alternative splicing event in the mutant transcript of the *Pkd1*^{del2–6} mice resulted in an mRNA lacking exons 2–7 and a subsequent frame shift leading to a stop codon early in exon 8, thus effectively creating a null allele. This finding is of clinical significance, suggesting ‘in-frame deletions’ may function as inactivation mutations. The PC1 protein was absent in the *Pkd1*^{del2–6} mouse kidneys, which is consistent with the mRNA data.

Although both new *Pkd1*^{del2–6} and the previously published *Pkd1*^{null9} mutations result in a null effect and the absence of PC1 protein, the main difference between them is the removal of the *neo* cassette in the *Pkd1*^{del2–6}-mutant allele. One striking phenotypic difference between homozygous *Pkd1*^{del2–6} and *Pkd1*^{null} mice that we observed was their survival rate. Approximately 55% of the *Pkd1*^{del2–6} homozygotes survived to term, although most died within hours after birth, whereas the *Pkd1*^{null} homozygotes rarely survived beyond E18.5, as reported previously.⁹ Only four of 143 *Pkd1*^{null} homozygotes in the C57/B6 genetic background survived to term, but died immediately after birth. Most *Pkd1*^{null} homozygous embryos with a C57BL/6–129 mixed background, identical to *Pkd1*^{del2–6}, succumbed by E17.5.⁹ *Pkd1*^{del2–6} and *Pkd1*^{null} kidneys both appear to be phenotypically normal until E15.5, when cysts first arise. Aside from the renal phenotype, *Pkd1*^{del2–6} mice develop pancreatic cystic disease, as well as gross edema, as reported previously for *Pkd1*^{null} mice.⁹ However, the observed phenotype in *Pkd1*^{del2–6} seems to be slightly milder than that observed in *Pkd1*^{null} mice likely contributing to the increased survival observed in the former. The insertion of a *neomycin* resistance cassette in exon 4 of the *Pkd1*^{null} mutants may have an impact on the genomic structure different from the

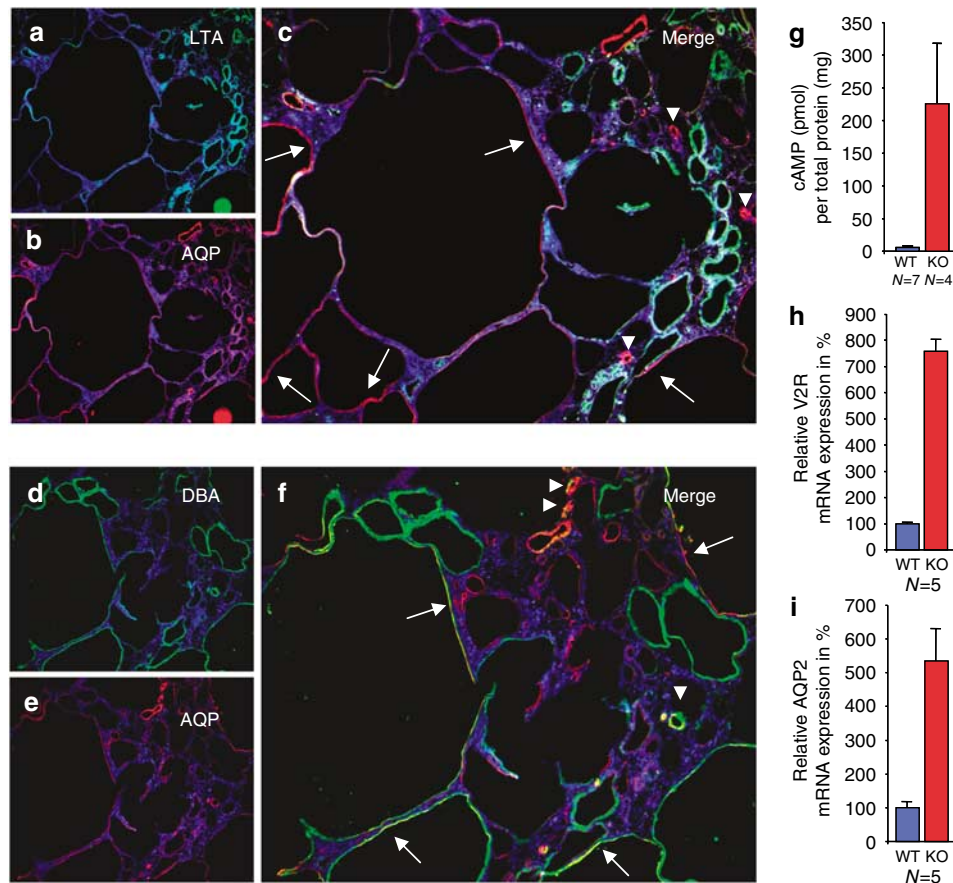


Figure 9 | Increased cAMP levels correlate with cystic disease progression in γ Gt.Cre:Pkd1^{lox/flox} mice. Co-staining for either LTA (a, c) or DBA (d, f) with AQP2 in normal-looking tubules. (b, c, e, f) shows predominantly apical presence of AQP2 in cysts of distal origin in P5 mice. Arrows indicate AQP2 in cysts, arrowheads indicate AQP2 in normal-looking tubules. (blue, DAPI; original magnification $\times 100$). (g) Direct measurement of cellular cAMP shows massive increase in cystic kidneys versus normal controls. (h, i) Real-time PCR showing large increase of both V2R (h) and AQP2 (i) mRNA in cystic kidneys of P19 γ Gt.Cre:Pkd1^{lox/flox} mice.

deletion of exons 2–6 in the *Pkd1*^{del2-6} mutants, which may contribute to the increased survival of *Pkd1*^{del2-6}. We did not observe any abnormality in the left–right body axis determination in all 41 *Pkd1*^{del2-6} homozygous embryos examined (out of a total of 323 pups in 46 litters). In *Pkd1*^{del2-6/+} mice 8–21 months old, we observed sporadic macroscopic liver and kidney cysts.

A new ADPKD mouse model by somatic inactivation of the normal *Pkd1* allele

In 1992, Reeders⁴ proposed a two-hit hypothesis as the mechanism of cystogenesis for sporadic distribution of cysts observed in ADPKD, and experimental evidence in human tissues has supported this notion.^{5,6} To study the effect of somatic inactivation of the *Pkd1* allele in an animal heterozygous for a *Pkd1*^{null} mutation, we generated a compound heterozygous *Pkd1*-knockout mouse, γ Gt.Cre:Pkd1^{null/flox}. Characterization of this model clearly demonstrated that somatic inactivation of the second (normal) *Pkd1* allele causes cystogenesis, in accordance with the two-hit hypothesis. The massive cystogenesis in γ Gt.Cre:Pkd1^{null/flox} mice, as compared with the very mild

phenotype in *Pkd1*^{del2-6/+} mice and other reported heterozygous phenotype in *Pkd1* mutants, can be attributed to the much higher rate of second hits due to the presence of a *Cre* transgene and the inactivation of the second *Pkd1* allele due to the recombination of the loxP sites rather than awaiting spontaneous events. Recently, Piontek *et al.*¹⁵ reported the creation of a conditional *Pkd1*-knockout model in which somatic inactivation of *Pkd1* was achieved by *Cre* expression under an mouse mammary tumor virus (MMTV) promoter. However, cysts developed and progressed very slowly. Very few renal cysts formed in mice older than 2.5 months,¹⁵ probably because of a mosaic low level of expression of *Cre* recombinase. The very sporadic cyst formation and slow progression, although mimicking the ADPKD phenotype, makes this model less desirable for the study of cystogenesis. In the γ Gt-driven model discussed in this study, we report massive and rapidly progressing cystogenesis in postnatal animals, which would be a very useful tool for further studies of polycystin function and ADPKD.

A notable observation during characterization of the γ Gt.Cre:Pkd1^{null/flox} phenotype was that the larger cysts appeared to be primarily located in the renal medulla,

indicating a more distal origin. γ Gt.Cre was previously reported to be expressed in renal cortex, which mostly consists of proximal tubules.¹⁹ This study identified a broader expression pattern for γ Gt.Cre, which raises several new questions. Is γ Gt.Cre expressed developmentally in common tubule progenitor cells that later develop into distinct tubular segments? Timed pregnancies using *DsRed*-reporter mice showed no evidence of γ Gt.Cre expression at E15.5 (data not shown), suggesting this is not a likely possibility. A more favorable explanation is that γ Gt.Cre is expressed in distal tubule segments at a low level as only four Cre molecules are necessary for the excision of the floxed fragment.^{21,22} The use of *DsRed*-reporter mice in conjunction with DBA, a collecting-duct marker, revealed the presence of Cre recombinase in distal segment derived cyst-lining epithelia, which indicates that the γ Gt promoter fragment was indeed active in distal nephron segments. Staining with other tubular markers, such as THP, further confirmed this observation, suggesting that this model is of close resemblance to human ADPKD in which cysts are of both distal and proximal tubule origin.²³

Another interesting observation is that some cysts are positive for THP, DBA, and LTA markers in γ Gt.Cre:*Pkd1*^{flox/flox} animals under postnatal 2 weeks of age. In wild-type animals, this is only observed in embryonic kidneys. Because expression of multiple tubular segmental markers was not seen in older γ Gt.Cre:*Pkd1*^{flox/flox} animals, these findings suggest a delay in the maturation of tubular epithelial cells in polycystic kidneys. Expression of the mesenchymal marker smooth-muscle actin in DBA- and THP-positive cysts supports this hypothesis (Figure S1).

Potential mechanisms for a faster growth rate in cysts derived from distal nephron segments

Cysts of distal tubule origin always appeared to be larger than those derived from proximal tubules, which is similar to what is observed in end-stage ADPKD kidneys in humans. We therefore investigated the possible relationship between cyst progression and tubular origins in time. Surprisingly, we found that at early stages (≤ 4 days), distal tubule cysts are, on average, already four times larger than their proximal counterparts. At late stages, the size ratio between DBA:LTA cysts increased up to 70-fold. Is the faster growth rate of distal cysts due to an increase in apoptosis in proximal versus distal nephron segments, or a higher rate of cell proliferation in the distal tubules? Although we observed enhanced apoptosis in γ Gt.Cre:*Pkd1*^{flox/flox} mouse kidneys, when compared with controls, by TUNEL and Casp3 staining, which label fragmented DNA in apoptotic cells and cells committed to apoptosis, respectively, we did not see any difference in cell death rate between cysts of proximal or distal tubule origin. In contrast, by proliferating-cell nuclear antigen staining, we observed a higher rate of proliferation in distal nephron segments when compared with proximal segments, which suggests that increased proliferation contributes to the more rapid growth of distal cysts in γ Gt.Cre:*Pkd1*^{flox/flox} mouse kidneys.

It is interesting to note that distal segments (positive for DBA) and medullary nephron segments seem to have a higher proliferation rate than proximal tubules in normal early postnatal kidneys (Figure 8). Moreover, the size of proximal tubule cysts ceased to increase from postnatal day 12–15 (Figure 6), which coincides with the completion of development and maturation of the normal kidney. After this time, the proximal tubule cysts were significantly smaller, which may be an indication of a non-essential role of PC1 in this nephron segment from this stage onwards. This notion is supported by our previous finding that expression of PC1 in the kidney decreases drastically after postnatal 2 weeks.²⁴ Particularly, proximal tubule expression of PC1 became nearly undetectable in mature kidneys.²⁵ In the context of the ‘flow hypothesis’, microvilli have been proposed to act as flow sensors in the proximal tubules,²⁶ which could compensate for the loss of *Pkd1* as a flow sensor.² The distal tubules lack this ameliorating system, indicating that *Pkd1* might have a critical role in the maintenance of tubule diameter in distal tubules. Alternatively, the interstitial spaces adjacent to distal tubules might be more prone to alteration or injury than those adjacent to proximal tubules.²⁷

Increased intracellular cAMP level has been seen in human end-stage ADPKD kidneys and may play an important role in cyst progression.^{28–32} Since camp-responsive proteins, such as V2R and AQP2, are exclusively present in the distal segments of the kidney and increased water secretion could contribute to the faster growth rate of distal cysts. Therefore, we determined the localization of AQP2 in γ Gt.Cre:*Pkd1*^{flox/flox} mutants. As expected, AQP2 translocated to the apical membrane in distal cysts labeled by DBA, although remaining in its intracellular location in normal-looking tubules as shown in Figure 9. We also determined the mRNA expression levels in cystic kidneys for AQP2 and V2R, and observed a 5- and 7-fold increase, respectively. Direct measurements of cellular cAMP levels in γ Gt.Cre:*Pkd1*^{flox/flox} and their normal littermates detected a > 20 -fold increase in cystic kidneys, thus providing the first conclusive evidence for an increase of cAMP in a *Pkd1*-disease model and its potential contribution to cyst enlargement.

In summary, the rapidly progressing polycystic kidney phenotype in our γ Gt.Cre:*Pkd1*^{null/flox} and γ Gt.Cre:*Pkd1*^{flox/flox} mutants, with its massive cystogenesis at an early age, but without negative effects on embryonic development, provides us with an excellent animal model for studies of pathogenesis and intervention of ADPKD.

MATERIALS AND METHODS

Generation of the *Pkd1*-targeting construct and chimeric mice

A neomycin selection cassette flanked by two loxP sites was inserted into the *EcoRI* site, located 1.2 kb upstream of exon 2. A third loxP site was inserted into intron 6. All three loxP sites in the targeting vector are in a direct repeat configuration. Chimeric mice were generated by transfecting embryonic stem cells (E14, 129/sv background) with the targeting vector, and homologous recombinants were identified by PCR and Southern blot analysis using a

5' probe, consisting of a 1-kb PCR fragment located ~1 kb upstream of the *AvrII* restriction site between exon 1 and 2 (Figure 1a, probe A). Two independently targeted embryonic stem cell clones were injected into C57BL/6J blastocysts to generate chimeric mice. Chimeric mice were identified by contribution of the embryonic stem cells to coat color (agouti) and were bred with wild-type C57BL/6 mice to demonstrate germline transmission. *DsRed* mice (STOCK Tg(ACTB-*DsRed*.MST)1Nagy/J) were obtained from Jackson Laboratories (Bar Harbor, ME, USA).

Primers used

Recombination PCR was performed with the following primers: exon 1-forward (KO-F): cgagtctgcatcc; exon 9-reverse (R104): caggctctcaagcttctgg; exon 2-forward (F27): ctcagacgtggacatag; exon5-reverse, (R37): ttgcttacttgacactctg; exon 10-forward (F201): tgtgtgcctgaggaactctg; exon 11-reverse (R201): ccaggggacactg taggaga; 'Flox' PCR was performed with the following primers: LoxP-forward (mPKD1loxpin6): acattatacgaagtattcatatgcttg; WT-forward (mPKD1in6Spe2): gtctcctgacaggactagtctt; intron 7-reverse (mPKD1WTR1): cccctctcatctgtttcct; *Cre*-PCR was performed with the following primers: γ GT.*Cre*-forward (PST-N10-F): cttctccagctcc cctctgtgttt; γ GT.*Cre*-reverse (PST-N10-R): ccgcgcctgaagatataga.

(Reverse transcriptase)-PCR conditions

Total RNA was harvested from kidney tissues using Trizol™ (Invitrogen, Carlsbad, CA, USA) according to the supplier's protocol. RNA quality and concentration were assayed using agarose gel electrophoresis and UV spectrophotometry (A_{260}/A_{280}). A 5- μ g weight of total RNA was reverse transcribed using Superscript™ II reverse transcriptase (Invitrogen) in the presence of RNaseOUT™ ribonuclease inhibitor (Invitrogen).

Reverse transcription reactions were performed according to the manufacturer's protocol (Invitrogen). Basic PCR conditions were as follows: (1) 94 °C, 4 min; (2) 94 °C, 1 min; (3) 60 °C, x min; (4) 72 °C, 1 min; and (5) 72 °C, 10 min. Where x depends on the expected product length (generally 1 min kb⁻¹) and steps 2-4 are repeated for 30-35 cycles on a PTC-200 thermal cycler (MJ Research, Waltham, MA, USA).

Real-time PCR

Samples were prepared using the Quantitect SYBR green kit (Qiagen, Valencia, CA, USA) according to the manufacturer's protocol and semi-quantitative real-time PCR for AQP2 and V2R was performed with a Lightcycler 1 (Roche, Nutley, NJ, USA) with glyceraldehyde-3-phosphate dehydrogenase (*Gapdh*) as internal control. The following primer sets for mouse *Aqp2* (GenBank NM009699), *V2R* (GenBank NM019404), and *Gapdh* (GenBank M32599) were designed with Vector NTI advance software (Invitrogen) using identical criteria: *Aqp2*: 5'-ATGTGGGAACTCCGGTCCAT; 3'-CAATCTGGAGCACAGAGGGTG; *V2R*: 5'-ATGATCCTGGTGTCTACCACGT; 3'-ACTAACAGCGGGTCTCGGTC; and *Gapdh*: 5'-GATGCCCCATGTTTGTGAT; 3'-TTGTCATGGATGACCTTGGC.

Real-time PCR was performed using the following temperature profile: denaturation: 95 °C for 15 min; cycling: melt 94 °C for 15 s; annealing: 53 °C for 8 s; extension: 72 °C for 8 s.

Melting-curve analysis was performed after each run and data were analyzed using Roche Lightcycler data analysis software (v3.5.28). ΔC_T values for *Aqp2*, *V2R*, and *Gapdh* were determined using second-derivative analysis of the amplification curves. ΔC_T for *Gapdh* was used to normalize data (subtracting *Gapdh* ΔC_T from

ΔC_T for *Aqp2* and *V2R*) and final results were expressed as a % compared with control.

cAMP measurements

Kidneys from 19-day-old wild-type and CKO mice were harvested and subsequently homogenized in 0.1 M HCl. Total cyclic was measured in the resulting lysates using an enzymatic immunoassay (Sigma, St Louis, MO, USA) according to the manufacturer's protocol. The assay is based on competition between unlabeled cAMP and peroxidase-labeled cAMP for a limited number of sites on an immobilized cAMP-specific antibody. The amount of peroxidase-labeled ligand bound by the antibody is inversely proportional to the concentration of unlabeled cAMP. Standard curves were generated for each experiment.

Western blot analysis

Western blotting was performed as previously described.¹⁸ The primary antibodies used included rabbit anti-PC2 polyclonal antibody 96525,³³ rabbit anti-PC1 polyclonal antibody 96521, rabbit anti-p21 polyclonal antibody (Santa Cruz Biotechnology, Santa Cruz, CA, USA), rabbit anti-p27 polyclonal antibody (Santa Cruz Biotechnology), and mouse anti-PC1 monoclonal antibody (7e12; a kind gift from Dr C Ward). The secondary antibody used for western blotting was goat anti-rabbit IgG-horseradish peroxidase or goat-anti-mouse IgG-horseradish peroxidase, 1:10 000 dilution (Amersham Biosciences, Pittsburgh, PA, USA).

Histology and immunocytochemistry

For histological studies, kidneys from study animals were hemisected in either sagittal or cross-sectional plane, fixed in 10% formalin, and embedded in paraffin. Sections were subsequently stained with hematoxylin-eosin.⁹ Immunofluorescence was performed as follows: formalin fixed, paraffin-embedded sections were deparaffinized with xylene and subsequently rehydrated with a graded series of alcohol solutions (100-30%). Antigen was retrieved with a commercial antigen-retrieval solution (Vector Laboratories, Burlingame, CA, USA) according to the manufacturer's protocol. Sections were blocked with 10% normal goat serum or 5% bovine serum albumin in phosphate-buffered saline (Dako, Carpinteria, CA, USA) for 30-60 min at room temperature.

Primary and secondary antibodies and/or lectins were applied diluted in either 2% goat serum/phosphate-buffered saline or 1% bovine serum albumin/phosphate-buffered saline, and incubated for 1 h at room temperature. Primary antibodies or lectins were used at the following dilutions: rhodamine-coupled DBA (Vector Laboratories) at 1:50 dilution; fluorescein-coupled LTA (Vector Laboratories) at 1:500 dilution; goat anti-THP/uromucoid IgG (Cappel/MP Biomedicals, Solon, OH, USA) at 1:100 dilution; mouse anti-smooth-muscle actin (Sigma) at 1:200 dilution; goat anti-AQP2 (Santa Cruz Biotechnology) at 1:100 dilution; rabbit anti-cleaved caspase3 (Cell Signaling, Danvers, MA, USA) at 1:400 dilution; fluorescein isothiocyanate-coupled rabbit anti-RFP (ab34764; Abcam, MA, USA) 1:500; Alexa 594-coupled donkey anti-mouse/anti-rabbit IgG's at 1:2000 dilutions. Sections were mounted in Vectashield + Dapi (Vector Laboratories). Epifluorescent images were taken with a Nikon Eclipse TE2000-E inverted microscope (Nikon, Melville, NJ, USA) equipped with a Photometrics Coolsnap HQ camera (Photometrics, AZ) and background subtraction and filtering were performed using Adobe Photoshop CS2 (Adobe Systems Inc., San Jose, CA, USA).

TUNEL staining of formalin-fixed, paraffin-embedded tissue sections was performed using the Apoptag, Peroxidase In Situ apoptosis Detection kit (Chemicon, CA, USA) according to the manufacturer's protocol, and light-microscopic images were taken with a Leica DMLS microscope (Leica Microsystems GmbH, Nussloch, Germany) equipped with a Kodak DC290 camera (Kodak, Rochester, NY, USA).

Digital analysis of cyst size

Paraffin sections were pretreated as described and subsequently co-stained with DBA and LTA. Epifluorescent images were taken at a total magnification of $\times 100$. At least four different fields per section were photographed, and cyst number and cyst area were measured using Image Pro Plus v5 software (Media Cybernetics, MD, USA), and numerical data were subsequently processed in Microsoft Excel.

ACKNOWLEDGMENTS

We thank Alex W Beck for technical assistance during this study. This work was supported by grants from the National Institutes of Health, DK-40703, DK-53357, DK-51050 (JZ), DK-46282 (EGN), and by a Polycystic Kidney Foundation Postdoctoral Fellowship to X Li and a postdoctoral fellowship from American Heart Association to A Takakura.

SUPPLEMENTARY MATERIAL

Figure S1. Evidence of a delay or defect in kidney maturation in γ Gt.Cre:Pkd1^{flox/flox} mice.

Figure S2. Increased apoptosis occurs in cystic kidneys of γ Gt.Cre:Pkd1^{flox/flox} mice in time.

REFERENCES

- Tahvanainen E, Tahvanainen P, Kaariainen H *et al.* Polycystic liver and kidney diseases. *Ann Med* 2005; **37**: 546–555.
- Nauli SM, Alenghat FJ, Luo Y *et al.* Polycystins 1 and 2 mediate mechanosensation in the primary cilium of kidney cells. *Nat Genet* 2003; **33**: 129–137.
- Nauli SM, Zhou J. Polycystins and mechanosensation in renal and nodal cilia. *Bioessays* 2004; **26**: 844–856.
- Reeders ST. Multilocus polycystic disease. *Nat Genet* 1992; **1**: 235–237.
- Qian F, Watnick TJ, Onuchic LF *et al.* The molecular basis of focal cyst formation in human autosomal dominant polycystic kidney disease type I. *Cell* 1996; **87**: 979–987.
- Watnick TJ, Torres VE, Gandolph MA *et al.* Somatic mutation in individual liver cysts supports a two-hit model of cystogenesis in autosomal dominant polycystic kidney disease. *Mol Cell* 1998; **2**: 247–251.
- Lu W, Peissel B, Babakhanlou H *et al.* Perinatal lethality with kidney and pancreas defects in mice with a targeted Pkd1 mutation. *Nat Genet* 1997; **17**: 179–181.
- Kim K, Drummond I, Ibraghimov-Beskrovnaya O *et al.* Polycystin 1 is required for the structural integrity of blood vessels. *Proc Natl Acad Sci USA* 2000; **97**: 1731–1736.
- Lu W, Shen X, Pavlova A *et al.* Comparison of Pkd1-targeted mutants reveals that loss of polycystin-1 causes cystogenesis and bone defects. *Hum Mol Genet* 2001; **10**: 2385–2396.
- Boulter C, Mulroy S, Webb S *et al.* Cardiovascular, skeletal, and renal defects in mice with a targeted disruption of the Pkd1 gene. *Proc Natl Acad Sci USA* 2001; **98**: 12174–12179.
- Wu G, D'Agati V, Cai Y *et al.* Somatic inactivation of Pkd2 results in polycystic kidney disease. *Cell* 1998; **93**: 177–188.
- Pennekamp P, Karcher C, Fischer A *et al.* The ion channel polycystin-2 is required for left-right axis determination in mice. *Curr Biol* 2002; **12**: 938–943.
- Lu W, Fan X, Basora N *et al.* Late onset of renal and hepatic cysts in Pkd1-targeted heterozygotes. *Nat Genet* 1999; **21**: 160–161.
- Araki K, Araki M, Miyazaki J *et al.* Site-specific recombination of a transgene in fertilized eggs by transient expression of Cre recombinase. *Proc Natl Acad Sci USA* 1995; **92**: 160–164.
- Piontek KB, Huso DL, Grinberg A *et al.* A functional floxed allele of Pkd1 that can be conditionally inactivated *in vivo*. *J Am Soc Nephrol* 2004; **15**: 3035–3043.
- Qian F, Germino FJ, Cai Y *et al.* PKD1 interacts with PKD2 through a probable coiled-coil domain. *Nat Genet* 1997; **16**: 179–183.
- Nadasdy T, Laszik Z, Lajoie G *et al.* Proliferative activity of cyst epithelium in human renal cystic diseases. *J Am Soc Nephrol* 1995; **5**: 1462–1468.
- Li X, Luo Y, Starremans PG *et al.* Polycystin-1 and polycystin-2 regulate the cell cycle through the helix-loop-helix inhibitor Id2. *Nat Cell Biol* 2005; **7**: 1102–1112.
- Iwano M, Plieth D, Danoff TM *et al.* Evidence that fibroblasts derive from epithelium during tissue fibrosis. *J Clin Invest* 2002; **110**: 341–350.
- Kaufman MH. *The Atlas of Mouse Development*. Academic Press: San Diego, CA, 1992, 512 pp, \$80. In (vol 37), 1994, p 120.
- Kilby NJ, Snaith MR, Murray JA. Site-specific recombinases: tools for genome engineering. *Trends Genet* 1993; **9**: 413–421.
- Martin SS, Pulido E, Chu VC *et al.* The order of strand exchanges in Cre-LoxP recombination and its basis suggested by the crystal structure of a Cre-LoxP Holliday junction complex. *J Mol Biol* 2002; **319**: 107–127.
- Devuyst O, Burrow CR, Smith BL *et al.* Expression of aquaporins-1 and -2 during nephrogenesis and in autosomal dominant polycystic kidney disease. *Am J Physiol* 1996; **271**: F169–F183.
- Geng L, Segal Y, Pavlova A *et al.* Distribution and developmentally regulated expression of murine polycystin. *Am J Physiol* 1997; **272**: F451–F459.
- Geng L, Segal Y, Peissel B *et al.* Identification and localization of polycystin, the PKD1 gene product. *J Clin Invest* 1996; **98**: 2674–2682.
- Du Z, Yan Q, Duan Y *et al.* Axial flow modulates proximal tubule NHE3 and H-ATPase activities by changing microvillus bending moments. *Am J Physiol Renal Physiol* 2006; **290**: F289–F296.
- Alcorn D, Emslie KR, Ross BD *et al.* Selective distal nephron damage during isolated kidney perfusion. *Kidney Int* 1981; **19**: 638–647.
- Gattone II VH, Wang X, Harris PC *et al.* Inhibition of renal cystic disease development and progression by a vasopressin V2 receptor antagonist. *Nat Med* 2003; **9**: 1323–1326.
- Marfella-Scivittaro C, Quinones A, Orellana SA. cAMP-dependent protein kinase and proliferation differ in normal and polycystic kidney epithelia. *Am J Physiol Cell Physiol* 2002; **282**: C693–C707.
- Orellana SA, Marfella-Scivittaro C. Distinctive cyclic AMP-dependent protein kinase subunit localization is associated with cyst formation and loss of tubulogenic capacity in Madin-Darby canine kidney cell clones. *J Biol Chem* 2000; **275**: 21233–21240.
- Mangoo-Karim R, Uchic ME, Grant M *et al.* Renal epithelial fluid secretion and cyst growth: the role of cyclic AMP. *FASEB J* 1989; **3**: 2629–2632.
- Grantham JJ, Mangoo-Karim R, Uchic ME *et al.* Net fluid secretion by mammalian renal epithelial cells: stimulation by cAMP in polarized cultures derived from established renal cells and from normal and polycystic kidneys. *Trans Assoc Am Phys* 1989; **102**: 158–162.
- Li X, Luo Y, Starremans PG *et al.* Polycystin-1 and polycystin-2 regulate the cell cycle through the helix-loop-helix inhibitor Id2. *Nat Cell Biol* 2005; **7**: 1102–1112.